Modified hybrid closure approximation for prediction of flow-induced fiber orientation

Kyeong-Hee Han and Yong-Taek Im[a)]

Computer Aided Materials Processing Laboratory, Department of Mechanical Engineering, ME3227, Korea Advanced Institute of Science and Technology, 373-1 Kusong-dong, Yusong-gu Taejon 305-701, South Korea

(Received 8 July 1998; final revision received 25 January 1999)

Synopsis

Distribution of fiber orientation in flow molding processes with short-fiber reinforcements is of great importance because it affects the mechanical properties of molded parts. Due to trade-off between the computational efficiency and accuracy, a second-order orientation tensor has been widely used to describe the fiber orientation distribution. For calculation of this fiber orientation tensor, a closure approximation has been introduced to reduce a higher fourth-order orientation tensor to a lower second order. In the present investigation, a hybrid closure approximation has been modified. Two parametric forms of the distribution function, which accurately describe the random-in-space, random-in-plane, and uniaxial distributions of the fiber orientation were linearly interpolated. The interpolating factor was obtained as a function of the fiber interaction coefficient by fitting the distribution function calculations. Test simulation in homogeneous flow and nonhomogeneous flow fields, respectively, showed that the proposed closure approximation gives good performance for a wide range of C_I values without showing nonphysical behavior. © *1999 The Society of Rheology.* [S0148-6055(99)01603-X]

I. INTRODUCTION

The fiber orientation distribution, which has a large effect on the mechanical properties of the short-fiber-reinforced composite parts, greatly changes during processing. For effective production of such products via flow molding processes such as injection molding and compression molding, it is essential to predict the flow-induced variation of the fiber orientation distribution. The importance of the distribution of such a fiber orientation has led to many investigations.

Jeffery (1922) has derived the equation of orientation change of an ellipsoidal particle immersed in a homogeneous flow field based on hydrodynamics. Folgar and Tucker (1984) have suggested a phenomenological model of rotary diffusivity to consider the change in orientation caused by fiber–fiber interactions. Since numerous short fibers exist in molded parts, it is impossible to consider fibers individually. Thus, the orientation distribution function (ODF), which is a probability density function of the fiber orientation, was introduced to fully describe the fiber orientation distribution in three dimensions. Adopting the ODF description in numerical simulations requires a tremendous amount of calculations since hundreds of degrees of freedom must be considered at each spatial point.

[a)]Author to whom all correspondence should be addressed. Electronic mail: ytim@convex.kaist.ac.kr

For more efficient numerical simulation of the orientation state of fibers, Advani and Tucker (1987) have made use of the orientation tensor which was originally introduced by Hand (1962). In this approach, only a few components are required to represent the state of orientation at each spatial point. This advantage has allowed the orientation tensor, especially the second-order tensor, to be widely used in the calculation of fiber orientation in flow molding processes [Altan *et al.* (1990); Bay and Tucker (1992a,b), de Frahan *et al.* (1992); Gupta and Wang (1993); Ranganathan and Advani (1993); Tucker and Advani (1994); Chung and Kwon (1995); Ko and Youn (1995)]. A weakness of the orientation tensor approach is that a fourth-order tensor must be approximated by a known second-order tensor in solving the governing equations. This closure approximation problem arises in many areas such as polymer dynamics and liquid-crystalline dynamics where the time evolution equation for the probability density is expressed in terms of moments.

So far, the hybrid closure approximation proposed by Advani and Tucker (1987, 1990) has most widely been used in the simulation of fiber orientations, since it is able to predict the trends of orientation distribution fairly well and can easily be implemented into numerical calculations. However, the involved numerical error is not negligible for some cases according to Bay and Tucker (1992b). They concluded that for a quantitative agreement between simulations and experiments an improved closure approximation is required.

For this purpose, several approaches have been introduced. Bay (1991) proposed a closure approximation based on the work by Hand (1962) by fitting steady-state orientation distributions for a simple shear flow. Verley and Dupret (1993) proposed a natural closure approximation, a polynomial function of the second-order orientation tensor, which agrees with the analytic solutions of the ODF when assuming no fiber–fiber interactions. Cintra and Tucker (1995) proposed an orthotropic fitted closure approximation in which three independent terms of the fourth-order orientation tensor were selected by assuming orthotropy. These terms were determined by fitting polynomial functions with numerical calculations of the ODF for selected flow fields. Schieber (1993) and Chaubal and Leal (1998) introduced parametric density estimation approach for microstructured fluids in which a closure equation was constructed by proposing a parametric form of the ODF. This approach has an advantage over the previous curve fitting approaches in that it automatically satisfies the important properties of the closure equation. Considering the accuracy, however, it is less accurate than the fitting approach in general.

In the present investigation, both the parametric density estimation and the fitting approach were adopted to construct a new closure approximation in which two forms of the ODF were interpolated by applying the fitting with distribution function calculations. This closure approximation accurately describes the random-in-space, random-in-plane, and uniaxial distributions of the fiber orientations, whereas the hybrid closure approximation accurately describes the random-in-space and uniaxial distributions.

For verification, the predicted fiber orientation distribution using the second-order orientation tensor equation was compared to analytic and numerical solutions of the ODF. For numerical calculations of the ODF, finite-element formulations were carried out and calculations were performed using four different values of the fiber–fiber interaction coefficient in various flow fields to ensure the generality and stability of the proposed closure approximation.

II. FIBER ORIENTATION

A. Description of fiber orientation

The orientation of a single short fiber can be represented by the unit vector **p** shown in Fig. 1. Components of the vector **p** are described by the angles θ and ϕ as follows:

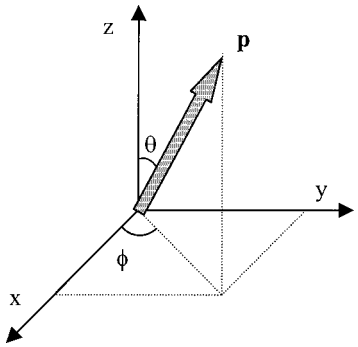

FIG. 1. Orientation of a single fiber described by the unit vector **p**.

$$\mathbf{p} = (p_1, p_2, p_3) = (\sin\theta\cos\phi,\ \sin\theta\sin\phi,\ \cos\theta). \tag{1}$$

Describing the orientation by individual fibers is ineffective since composites contain numerous fibers which invoke difficulties in calculating the anisotropy induced by fiber orientation. Thus, the concept of probabilistic distribution is usually applied. The orientation distribution function ψ is defined as a probability density function of fiber orientation as follows:

$$\psi(\mathbf{p}) = \psi(\theta,\phi) \equiv \lim_{\delta\theta,\delta\phi \to 0} P(\theta \leqslant \theta^* \leqslant \theta+\delta\theta,$$

$$\phi \leqslant \phi^* \leqslant \phi+\delta\phi)/(\sin\theta\delta\theta\delta\phi). \tag{2}$$

From this definition, the ODF satisfies the following properties:

$$\psi(\mathbf{p}) = \psi(-\mathbf{p}), \quad \text{or} \quad \psi(\theta,\phi) = \psi(\pi-\theta,\pi+\phi), \tag{3}$$

$$1 = \oint_S \psi(\mathbf{p})dA = \int_{\theta=0}^{\pi}\int_{\phi=0}^{2\pi} \psi(\theta,\phi)\sin\theta d\phi d\theta, \tag{4}$$

where, S denotes the surface of a unit sphere.

In order to use the ODF description in numerical calculations, a great deal of effort is required to consider the ODF values in every direction at each spatial point. The orientation tensor, defined in the following manner, can greatly reduce such efforts:

$$\text{second-order tensor:} \quad a_{ij} = \oint_S p_i p_j \psi dA, \tag{5}$$

$$\text{fourth-order tensor:} \quad a_{ijkl} = \oint_S p_i p_j p_k p_l \psi dA. \tag{6}$$

By definition, orientation tensors are symmetric in their indices and have the following normalized properties:

$$a_{kk} = 1, \tag{7}$$

$$a_{ijkk} = a_{ij}, \tag{8}$$

where repeated indices indicate summation unless otherwise specified. These properties give the second-order orientation tensor five independent components to be considered.

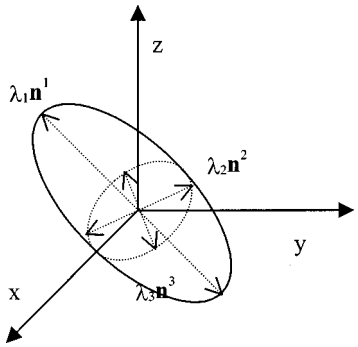

FIG. 2. Schematic representation of orientation distribution by the second-order orientation tensor.

Thus, the second-order orientation tensor can effectively describe various fiber orientation distributions using minimum information. The fiber orientation distribution can be visualized by using eigenvalues λ_i and eigenvectors $\mathbf{n}^i$ of the second-order orientation tensor as shown in Fig. 2.

B. Rate of change of fiber orientation

For description of the motion of a single fiber, all current models employ some form of the following equation:

$$\dot{p}_i = -\frac{1}{2}\omega_{ij}p_j + \frac{1}{2}\lambda(\dot{\gamma}_{ij}p_j - \dot{\gamma}_{kl}p_k p_l p_i) - \frac{D_r}{\psi}\frac{\partial \psi}{\partial p_i}, \tag{9}$$

where $\omega_{ij} = \partial v_j/\partial x_i - \partial v_i/\partial x_j$, and $\dot{\gamma}_{ij} = \partial v_j/\partial x_i + \partial v_i/\partial x_j$ are components of the vorticity and rate of deformation tensors, respectively, with $\partial/\partial p_i$ being the gradient operator on the surface of a unit sphere. λ is a shape factor of the fiber particle defined as $\lambda \equiv (r_e^2-1)/(r_e^2+1)$. As can be seen, it attains values between 0 (sphere) and 1 (infinitely slender), depending on a function of the aspect ratio. D_r is the effective diffusivity that accounts for interactions among fibers. If $D_r = 0$, Eq. (9) becomes identical to Jeffery's equation. In order to consider fiber–fiber interactions in nondilute suspensions, Folgar and Tucker's phenomenological model, $D_r = C_I\dot{\gamma}$, was used. In this model, C_I is the interaction coefficient and $\dot{\gamma} = \sqrt{(\dot{\gamma}_{ij}\dot{\gamma}_{ij})/2}$ is an effective shear rate.

Regarding the rate of change of the ODF, the following continuity equation is obtained by assuming ψ to be a convected quantity:

$$\frac{D\psi}{Dt} = -\frac{\partial}{\partial p_i}(\psi \dot{p}_i), \tag{10}$$

where, D/Dt denotes the material time derivative.

Finally, taking the material time derivative of Eq. (5) and incorporating Eqs. (9) and (10), the equation of change of the second-order orientation tensor can be obtained as

$$\frac{Da_{ij}}{Dt} = -\frac{1}{2}(\omega_{ik}a_{kj} - a_{ik}\omega_{kj}) + \frac{1}{2}\lambda(\dot{\gamma}_{ik}a_{kj} + a_{ik}\dot{\gamma}_{kj} - 2\dot{\gamma}_{kl}a_{ijkl}) + 2C_I\dot{\gamma}(\delta_{ij} - 3a_{ij}). \tag{11}$$

To solve this equation, the fourth-order orientation tensor a_{ijkl} must be approximated as a function of the second-order orientation tensor a_{ij}. As can be intuitively sensed, this closure approximation has a critical effect on the solution accuracy of Eq. (11).

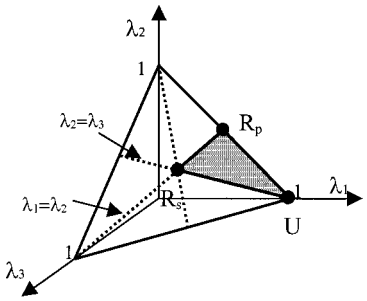

FIG. 3. Available region of eigenvalues in the $\lambda_1+\lambda_2+\lambda_3 = 1$ plane.

III. CLOSURE APPROXIMATION

The most frequently used closure approximation to date is the following hybrid closure approximation (HYB) proposed by Advani and Tucker (1987):

$$a_{ijkl}^{\mathrm{HYB}} = (1-f)a_{ijkl}^{\mathrm{LIN}} + f a_{ijkl}^{\mathrm{QUA}}, \tag{12}$$

where

$$a_{ijkl}^{\mathrm{LIN}} = \tfrac{1}{7}(a_{ij}\delta_{kl}+a_{ik}\delta_{jl}+a_{il}\delta_{jk}+a_{kl}\delta_{ij}+a_{jl}\delta_{ik}+a_{jk}\delta_{il}) - \tfrac{1}{35}(\delta_{ij}\delta_{kl}+\delta_{ik}\delta_{jl}+\delta_{il}\delta_{jk}), \tag{13}$$

$$a_{ijkl}^{\mathrm{QUA}} = a_{ij}a_{kl}, \tag{14}$$

and $f = 1-27\det(a_{ij})$.

This hybrid closure approximation accurately describes fiber orientation for random-in-space and uniaxial distributions and, in general, shows similar trends with the actual fiber orientation distribution observed in experiments. However, comparison with the distribution function calculation shows that the involved error is not always negligible.

Since a closure approximation cannot exactly describe all situations of the fiber orientation distribution, it is important to select reference flow fields that will guarantee the smallest error for general cases of interest. In this investigation, a new closure approximation is proposed for obtaining improved results of numerical calculations of the fiber orientation distribution during flow molding processes.

For simplification, the problem was considered in the principal coordinate system of a_{ij}. If λ_i and $\mathbf{n}^i = (n_1^i, n_2^i, n_3^i)$ are the ith eigenvalue and is the ith eigenvector, respectively, the second- and fourth-order orientation tensors denoted by b_{ij} and b_{ijkl} can be represented in this coordinate system as follows:

$$b_{ij} = n_o^i n_p^j a_{op} = \lambda_i \delta_{ij}, \text{ (no summation on } i) \quad \text{and} \tag{15}$$

$$b_{ijkl} = n_o^i n_p^j n_q^k n_r^l a_{opqr}. \tag{16}$$

Without loss of generality, the values of λ_i $(i = 1,2,3)$ lie in the shaded region of Fig. 3 with restriction of $\lambda_1 \geqslant \lambda_2 \geqslant \lambda_3$. At the three extremity points R_s, R_p, and U, the eigenvalues become

$$\text{at } R_s: \quad \lambda_1 = \lambda_2 = \lambda_3 = 1/3,$$

$$\text{at } R_p: \quad \lambda_1 = \lambda_2 = 1/2, \quad \lambda_3 = 0, \quad \text{and}$$

$$\text{at } U: \quad \lambda_1 = 1, \quad \lambda_2 = \lambda_3 = 0. \tag{17}$$

At R_s, various orientation distributions are possible, but in actual situations the most likely case is the random-in-space distribution. Similarly, R_p and U were assumed to represent random-in-plane and uniaxial distributions, respectively. These assumptions lead to the following nonzero components of b_{ijkl} at each extremity point:

$$\text{at } R_s: \quad b_{1111} = b_{2222} = b_{3333} = 1/5, \quad b_{2233} = b_{1133} = b_{1122} = 1/15,$$

$$\text{at } R_p: \quad b_{1111} = b_{2222} = 3/8, \quad b_{1122} = 1/8, \quad \text{and}$$

$$\text{at } U: \quad b_{1111} = 1. \tag{18}$$

The main assumption of the current closure approximation to be applied to general cases of the fiber orientation distribution is that the conditions at these three extremities must be satisfied. This closure approximation will be defined as the modified hybrid closure approximation.

A. Modified hybrid closure approximation: Model I

The modified hybrid closure approximation, model I, was defined to satisfy Eq. (18) by assuming the appropriate orientation distribution that exactly describes the conditions at the three extremities. It is reasonable to expect the orientation distribution to be expressed as simply as possible, e.g., egg like near R_s, disk like near R_p, and pen like near U. In this investigation, the following equations were assumed for each distribution:

$$\psi^{\text{egg}} = \alpha_1 r_1^2 + \alpha_2 r_2^2 + \alpha_3 r_3^2 \quad (\alpha_1 \geqslant \alpha_2 \geqslant \alpha_3 \geqslant 0), \tag{19}$$

$$\psi^{\text{disk}} = (1 - r_3^2)^k (\alpha_1 r_1^2 + \alpha_2 r_2^2) \quad (k \geqslant 0, \ \alpha_1 \geqslant \alpha_2 \geqslant 0), \quad \text{and} \tag{20}$$

$$\psi^{\text{pen}} = \alpha_1 (1 - r_3^2)^k r_1^{2m} \quad (k \geqslant 0, \ m \geqslant 1, \ \alpha_1 \geqslant 0), \tag{21}$$

where r_i are components of the orientation vector $\mathbf{p}$ in the direction of $\mathbf{n}^i$, and k, m, and α_i are parameters determined from a given a_{ij}. These ODFs are continuous in the following sense:

$$\psi^{\text{egg}}|_{\alpha_3 = 0} = \psi^{\text{disk}}|_{k = 0} \quad \text{and} \quad \psi^{\text{disk}}|_{\alpha_2 = 0} = \psi^{\text{pen}}|_{m = 1}. \tag{22}$$

In fact, ψ^{pen} can cover both disk- and egg-like regions if the condition of $m \geqslant 0$ is assumed. However, the combination of these three was employed since it is more physically meaningful and causes no notable differences in numerical results.

Since the ODF was defined to be symmetric in each coordinate plane, i.e., orthotropic, the fourth-order orientation tensor has six nonzero components, i.e., b_{1111}, b_{2222}, b_{3333}, b_{1122}, b_{1133}, and b_{2233}. Three of them, namely, b_{1111}, b_{2222}, and b_{3333} and their eigenvalues can be calculated in terms of k, m, and α_i as shown in Table I. From this, the relations between the second- and fourth-order orientation tensors can be derived as follows:

Egg like ($\lambda_3 \geqslant 1/5$):

$$b_{1111}^{\text{egg}} = \tfrac{3}{35}(10\lambda_1 - 1), \quad b_{2222}^{\text{egg}} = \tfrac{3}{35}(10\lambda_2 - 1), \quad \text{and} \quad b_{3333}^{\text{egg}} = \tfrac{3}{35}(10\lambda_3 - 1). \tag{23}$$

TABLE I. Principal components of the second- and fourth-order orientation tensors in terms of the parameters in Eqs. (19)–(21).

	Egg like	Disk like	Pen like
ODF (ψ)	$\alpha_1 r_1^2+\alpha_2 r_2^2+\alpha_3 r_3^2$	$(1-r_3^2)^k(\alpha_1 r_1^2+\alpha_2 r_2^2)$	$\alpha_1(1-r_3^2)^k r_1^{2m}$
		$1 = \beta_1+\beta_2$	
Normalization	$1 = \frac{4\pi}{3}(\alpha_1+\alpha_2+\alpha_3)$	$\beta_1 \equiv \left(\pi\int_0^{\pi}(\sin\phi)^{2k+3}d\phi\right)\alpha_1$	$1 = \left(\int_0^{2\pi}(\cos\theta)^{2m}d\theta\right)$
		$\beta_2 \equiv \left(\pi\int_0^{\pi}(\sin\phi)^{2k+3}d\phi\right)\alpha_2$	$\cdot\left(\int_0^{\pi}(\sin\phi)^{2k+2m+1}d\phi\right)\alpha_1$
λ_1	$\frac{4\pi}{15}(3\alpha_1+\alpha_2+\alpha_3)$	$\frac{2k+4}{4(2k+5)}(3\beta_1+\beta_2)$	$\frac{(2m+1)(2m+2k+2)}{(2m+2)(2m+2k+3)}$
λ_2	$\frac{4\pi}{15}(\alpha_1+3\alpha_2+\alpha_3)$	$\frac{2k+4}{4(2k+5)}(\beta_1+3\beta_2)$	$\frac{2m+2k+2}{(2m+2)(2m+2k+3)}$
λ_3	$\frac{4\pi}{15}(\alpha_1+\alpha_2+3\alpha_3)$	$\frac{\beta_1+\beta_2}{2k+5}$	$\frac{1}{2m+2k+3}$
b_{1111}	$\frac{4\pi}{35}(5\alpha_1+\alpha_2+\alpha_3)$	$\frac{(2k+4)(2k+6)}{8(2k+5)(2k+7)}(5\beta_1+\beta_2)$	$\frac{(2m+1)(2m+3)(2m+2k+2)(2m+2k+4)}{(2m+2)(2m+4)(2m+2k+3)(2m+2k+5)}$
b_{2222}	$\frac{4\pi}{35}(\alpha_1+5\alpha_2+\alpha_3)$	$\frac{(2k+4)(2k+6)}{8(2k+5)(2k+7)}(\beta_1+5\beta_2)$	$\frac{3(2m+2k+2)(2m+2k+4)}{(2m+2)(2m+4)(2m+2k+3)(2m+2k+5)}$
b_{3333}	$\frac{4\pi}{35}(\alpha_1+\alpha_2+5\alpha_3)$	$\frac{3(\beta_1+\beta_2)}{(2k+5)(2k+7)}$	$\frac{3}{(2m+2k+3)(2m+2k+5)}$

Disk like ($\lambda_3 \leqslant 1/5$, $\lambda_1 \leqslant 3\lambda_2$):

$$b_{1111}^{\text{disk}} = \frac{1-s}{8}(7\lambda_1-\lambda_2), \quad b_{2222}^{\text{disk}} = \frac{1-s}{8}(-\lambda_1+7\lambda_2), \quad \text{and} \quad b_{3333}^{\text{disk}} = (3s)\lambda_3,$$

$$\text{with } s = \lambda_3/(1+2\lambda_3). \tag{24}$$

Pen like ($\lambda_3 \leqslant 1/5$, $\lambda_1 \geqslant 3\lambda_2$):

$$b_{1111}^{\text{pen}} = (1-r)(1-s)\lambda_1, \quad b_{2222}^{\text{pen}} = (1-s)\lambda_2 - r(1-s)\lambda_1, \quad \text{and } b_{3333}^{\text{pen}} = (3s)\lambda_3,$$

$$\text{with } r = \lambda_2/(\lambda_1+3\lambda_2) \quad \text{and} \quad s = \lambda_3/(1+2\lambda_3). \tag{25}$$

Based on the normalized properties of Eq. (8), b_{2233}, b_{1133}, and b_{1122} can be determined as

$$b_{2233} = S-(\lambda_1-b_{1111}), \quad b_{1133} = S-(\lambda_2-b_{2222}), \quad \text{and} \quad b_{1122} = S-(\lambda_3-b_{3333}), \tag{26}$$

with $S = (1-b_{1111}-b_{2222}-b_{3333})/2$.

Thus, the modified hybrid closure approximation, model I, can be defined based on the above results as

$$a_{ijkl}^{\text{model I}} \equiv \begin{cases} a_{ijkl}^{\text{egg}} & \text{if} \quad \lambda_3 \geqslant 1/5 \\ a_{ijkl}^{\text{disk}} & \text{if} \quad \lambda_3 < 1/5, \lambda_1 \leqslant 3\lambda_2 \\ a_{ijkl}^{\text{pen}} & \text{if} \quad \lambda_3 < 1/5, \lambda_1 > 3\lambda_2 \end{cases}. \tag{27}$$

This equation is a continuous function of λ_i since it was based on a continuous ODF.

B. Modified hybrid closure approximation: Model II

As mentioned earlier, model I has an orthotropic property, and thus, is similar to the orthotropic closure approximation which was proposed by Cintra and Tucker (1995). They have proposed two kinds of closure approximations. Orthotropic fitted closure (ORF) is composed of polynomial functions of λ_i that were fitted to the numerical solutions of the ODF with $C_I = 0.01$ and $\lambda = 1$, and so, it does not explicitly satisfy the conditions at the three extremities. On the other hand, orthotropic smooth closure (ORS), which is described below, is a linear interpolation of the three special cases represented in Eq. (18). In this sense, it can be considered to be a kind of modified hybrid closure.

$$\begin{aligned} b_{1111}^{\text{ORS}} &= -0.15 + 1.15\lambda_1 - 0.10\lambda_2, \\ b_{2222}^{\text{ORS}} &= -0.15 + 0.15\lambda_1 + 0.90\lambda_2, \quad \text{and} \\ b_{3333}^{\text{ORS}} &= 0.60 - 0.60\lambda_1 - 0.60\lambda_2. \end{aligned} \tag{28}$$

The above results can be obtained by assuming the following parametric form of the distribution function:

$$\psi^{\text{ORS}}(\mathbf{r}) = \psi^{\text{ORS}}(\theta^*, \varphi^*) = \frac{\beta_1}{4\pi} + \frac{\beta_2}{2\pi}\delta\left(\theta^* - \frac{\pi}{2}\right) + \beta_3\delta\left(\theta^* - \frac{\pi}{2}\right)\delta(\varphi^*), \tag{29}$$

where, θ^* and φ^* are the angles of $\mathbf{r}$ as in Eq. (1) and $\delta(\cdot)$ is the delta function. The three parameters β_1, β_2, and β_3 can be easily obtained, respectively, from the definition of the orientation tensor as follows:

$$\beta_1 = 3\lambda_3, \quad \beta_2 = 2(\lambda_2 - \lambda_3), \quad \text{and} \quad \beta_3 = \lambda_1 - \lambda_2. \tag{30}$$

ORS and model I have the following properties for all λ_i:

$$b_{1111}^{\text{ORS}} > b_{1111}^{\text{model I}}, \quad b_{2222}^{\text{ORS}} > b_{2222}^{\text{model I}}, \quad \text{and} \quad b_{3333}^{\text{ORS}} > b_{3333}^{\text{model I}}. \tag{31}$$

This is evident from the definition of each distribution function. As will be discussed later, the b_{ijkl} values from the distribution function calculations (DFC) generally lie between those from model I and the ORS results. Therefore, a more accurate version of the modified hybrid closure approximation, model II, can be defined by combining model I and the ORS as

$$\psi^{\text{model II}} = (1 - \text{FAC}) \cdot \psi^{\text{model I}} + \text{FAC} \cdot \psi^{\text{ORS}}, \quad \text{or} \tag{32}$$

$$a_{ijkl}^{\text{model II}} \equiv (1 - \text{FAC}) \cdot a_{ijkl}^{\text{model I}} + \text{FAC} \cdot a_{ijkl}^{\text{ORS}}, \tag{33}$$

where FAC is an interpolating factor and can be determined by fitting the DFC results.

IV. CALCULATION OF ODF

In order to check whether the solution of Eq. (11) using the present modified closure approximation agrees with the exact solution of the orientation distribution, solutions of

the orientation distribution function are required. Hereafter, ''exact solutions'' or ''exact values'' will imply those obtained from the distribution function calculations. The material time derivative in Eq. (10) makes numerical calculations of the ODF nearly impossible if both space and time are considered. Therefore, in this investigation, exact solutions were calculated by analytic or numerical methods where material particles were followed in homogeneous flow fields.

A. Analytic solution

When $C_I = 0$, an analytic solution of the ODF is available since the orientation vector **p** can be expressed in terms of an initial vector and a velocity gradient. Applying the initial condition $p_i = q_i$ into Eq. (9) yields

$$p_i = \frac{E_{ik}q_k}{(E_{nl}q_lE_{nm}q_m)^{1/2}}, \tag{34}$$

where

$$\frac{DE_{ij}}{Dt} = \frac{1}{2}(-\omega_{ik}+\lambda\dot{\gamma}_{ik})E_{kj}, \tag{35}$$

and $E_{ij} = \delta_{ij}$ initially [Bretherton (1962)].

Since fibers in region $d\mathbf{q}$ are currently in region $d\mathbf{p}$, the ODF becomes

$$\psi(\mathbf{p}) = \psi_0(\mathbf{q})\frac{dA_q}{dA_p} = \psi_0(\mathbf{q})\frac{(E_{kl}q_lE_{km}q_m)^{3/2}}{\det(E_{ij})} = \psi_0(\mathbf{q})(\Lambda_{kl}p_l\Lambda_{km}p_m)^{-3/2}, \tag{36}$$

where $\Lambda_{ij} = E_{ij}^{-1}$.

From this, the second-order orientation tensor can be determined by [Altan and Rao (1995)]

$$a_{ij} = \oint_S p_ip_j\psi(\mathbf{p})dA_p = \oint_S \frac{E_{ik}q_kE_{jk}q_l}{E_{mn}q_nE_{mo}q_o}\psi_0(\mathbf{q})dA_q. \tag{37}$$

B. Numerical solution by the finite-element method

When $C_I \neq 0$, since an analytic solution is not available, the finite-element method was applied to solve the ODF numerically. Rearranging Eq. (10) with the use of Eq. (9) yields a differential equation of the ODF in the form of

$$\frac{D\psi}{Dt} = -\frac{\partial}{\partial p_i}\left(\psi\dot{p}_i^h - D_r\frac{\partial\psi}{\partial p_i}\right), \tag{38}$$

where

$$\dot{p}_i^h = -\tfrac{1}{2}\omega_{ij}p_j + \tfrac{1}{2}\lambda(\dot{\gamma}_{ij}p_j - \dot{\gamma}_{kl}p_kp_lp_i). \tag{39}$$

Multiplying both sides of Eq. (38) by the arbitrary function $\bar{\psi}$ and integrating over S, with special consideration of the gradient operator, yields

$$\oint_S \bar{\psi}\frac{D\psi}{Dt}dA = \oint_S \frac{\partial\bar{\psi}}{\partial p_i}\left(\psi\dot{p}_i^h - D_r\frac{\partial\psi}{\partial p_i}\right)dA. \tag{40}$$

Discretizing Eq. (40) with triangular elements, whose shape functions are $N_\alpha(\mathbf{p})$ ($\alpha = 1,2,3$), yields

$$m_{\alpha\beta}\frac{D\psi_\beta}{Dt} = k_{\alpha\beta}\psi_\beta(\alpha,\beta = 1,2,3), \tag{41}$$

where

$$m_{\alpha\beta} = \oint_S N_\alpha N_\beta dA, \tag{42}$$

$$k_{\alpha\beta} = \oint_S \frac{\partial N_\alpha}{\partial p_i}\left(N_\beta \dot{p}_i^h - D_r\frac{\partial N_\beta}{\partial p_i}\right)dA. \tag{43}$$

Representing the three nodal points of a triangular element ''*e*'' by $\mathbf{p}^1$, $\mathbf{p}^2$, and $\mathbf{p}^3$, the shape functions can be defined as

$$\begin{aligned} N_1(\mathbf{p}) &= (\mathbf{p}^{23}\times\mathbf{p}^{31})\times\mathbf{p}^{23}\cdot(\mathbf{p}-\mathbf{p}^2)/4A^2 \equiv \mathbf{c}_1\cdot\mathbf{p}+d_1, \\ N_2(\mathbf{p}) &= (\mathbf{p}^{31}\times\mathbf{p}^{12})\times\mathbf{p}^{31}\cdot(\mathbf{p}-\mathbf{p}^3)/4A^2 \equiv \mathbf{c}_2\cdot\mathbf{p}+d_2, \\ N_3(\mathbf{p}) &= (\mathbf{p}^{12}\times\mathbf{p}^{23})\times\mathbf{p}^{12}\cdot(\mathbf{p}-\mathbf{p}^1)/4A^2 \equiv \mathbf{c}_3\cdot\mathbf{p}+d_3, \end{aligned} \tag{44}$$

where, $\mathbf{p}^{\alpha\beta} = \mathbf{p}^\beta - \mathbf{p}^\alpha$ and A is the area of the triangular region Ω_e. From this, $m_{\alpha\beta}$ and $k_{\alpha\beta}$ can be derived as

$$m_{\alpha\beta} = \oint_{\Omega_e}(\mathbf{c}_\alpha\cdot\mathbf{p}+d_\alpha)(\mathbf{c}_\beta\cdot\mathbf{p}+d_\beta)dA, \tag{45}$$

$$k_{\alpha\beta} = \oint_{\Omega_e}(\mathbf{c}_\alpha\cdot\dot{\mathbf{p}}^h)(\mathbf{c}_\beta\cdot\mathbf{p}+d_\beta)dA - D_r\oint_{\Omega_e}\{(\mathbf{c}_\alpha\cdot\mathbf{c}_\beta)-(\mathbf{c}_\alpha\cdot\mathbf{p})(\mathbf{c}_\beta\cdot\mathbf{p})\}dA. \tag{46}$$

For numerical calculations, the surface of a unit sphere was discretized by 2700 triangular elements and the backward time derivative was employed with a time step of approximately $\Delta t = 0.1/\dot{\gamma}$ to ensure stability.

V. RESULTS AND DISCUSSION

In order to determine appropriate FAC values for the modified hybrid model II and to examine the validity of the proposed closure approximations, orientation calculations were performed for homogeneous flows. Calculations were also performed for nonhomogeneous flow fields to test the stability and generality of the current approximations. Since Folgar and Tucker's model $D_r = C_I\dot{\gamma}$ prevents relaxation of fiber orientation, calculation of the fiber orientation in start-up flow is considered in the present investigation. In all calculations, slender fibers ($\lambda = 1$) with initial random orientations were assumed.

A. Determination of FAC

Since the right side of governing Eq. (11) is a first degree homogeneous function of the velocity gradient, the time and velocity gradient can, respectively, be nondimensionalized as

TABLE II. Five representative flow fields for the verification study [Cintra and Tucker (1995)].

Flow field	Velocity field $(v_1/G, v_2/G, v_3/G)$
SS (simple shear)	$(x_2, 0, 0)$
SSA (shearing/stretching A)	$(-x_1+10x_2, -x_2, 2x_3)$
SSB (shearing/stretching B)	$(-x_1+x_2, -x_2, 2x_3)$
UE (uniaxial elongation)	$(2x_1, -x_2, -x_3)$
BE (biaxial elongation)	$(x_1, x_2, -2x_3)$

$$t^* = Gt \quad \text{and} \quad \left(\frac{\partial v_j}{\partial x_i}\right)^* = \frac{1}{G}\frac{\partial v_j}{\partial x_i}, \tag{47}$$

where, G represents an arbitrary constant of dimension t^{-1}.

In this investigation, calculations were made using these nondimensionalized variables and five representative flow fields were selected for the verification study as shown in Table II [Cintra and Tucker (1995)], where v_i/G is shown. Calculations of the orientation tensor were performed for C_I values ranging from 0 to 0.1 with the closure approximations as summarized in Table III.

For simple shear flow (SS), model I and ORS were applied directly to the exact solution of a_{ij} to estimate b_{ijkl} and compared with the exact solutions of b_{ijkl} as shown in Fig. 4. The comparison in Fig. 4(a) when $C_I = 0$ shows that the exact solution lies between the results of model I and ORS for the entire region. When $C_I = 0.1$, the comparison in Fig. 3(b) shows the same trend, but the exact solution can be seen to be closer to the results of model I. Similar trends could be observed for other flow fields and other C_I values. Such results show that the assumed parametric forms of $\Psi^{\text{model I}}$ and Ψ^{ORS} act as the lower and upper bounds, respectively, and therefore, it was construed that a combination of model I and ORS, if properly interpolated, would provide improved results.

To find the appropriate FAC for model II, numerical simulations were performed for all five flow fields with an assumed FAC value. The root-mean-square errors of all the nonzero components of b_{ijkl} were calculated for each flow field and the FAC was chosen to minimize the sum of those five or four error values depending on the amount of deviation. In Table IV, the determined FAC values are shown for selected C_I values. From these values, the FAC was approximated as a function of C_I as

$$\text{FAC} = 0.52 - 0.9655 \cdot C_I^{1/2} \quad (0 < C_I < 0.1). \tag{48}$$

TABLE III. Summary of closure approximations used in the current investigation.

Closure approximation	Source
HYB (hybrid)	Advani and Tucker (1987), Eq. (12)
ORS (orthotropic smooth)	Cintra and Tucker (1995), Eq. (28)
ORF (orthotropic fitted)	Cintra and Tucker (1995)
Model I (modified hybrid model I)	Eq. (27)
Model II (modified hybrid model II)	Eq. (33)

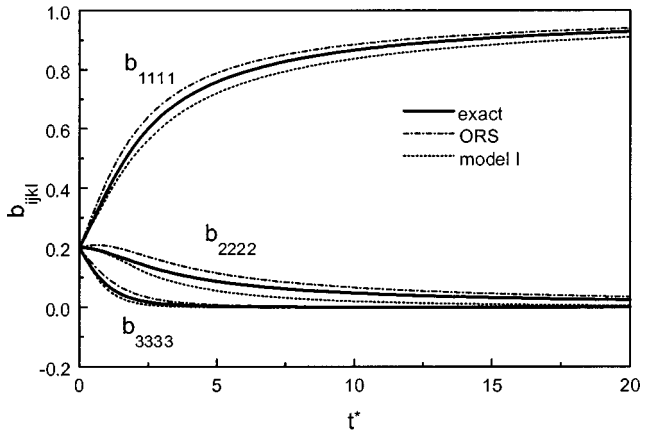

(a)

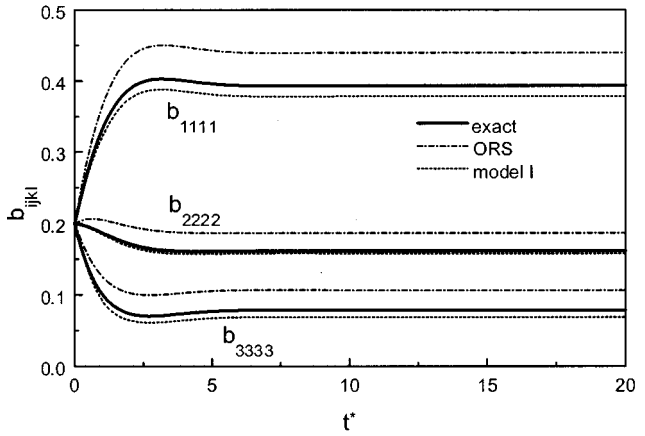

(b)

FIG. 4. Comparisons of b_{ijkl} between the exact solution and approximate values for a simple shear flow with (a) $C_I = 0$ and (b) $C_I = 0.1$.

B. Homogeneous flow fields

Comparisons of the calculation results using the five closure approximations as listed in Table II and the exact values are shown in Figs. 5(a) and 5(b) for the case of simple shear flow with $C_I = 0$ and $C_I = 0.01$, respectively. It can be seen that model II outperforms HYB, ORS, and model I as expected and nearly reproduces the exact values. It can be seen in Fig. 5(b) that model II and ORF make better predictions than the other

TABLE IV. FAC values determined for selected C_I values.

C_I	0.0	0.001	0.01	0.1
FAC	0.52	0.49	0.42	0.22

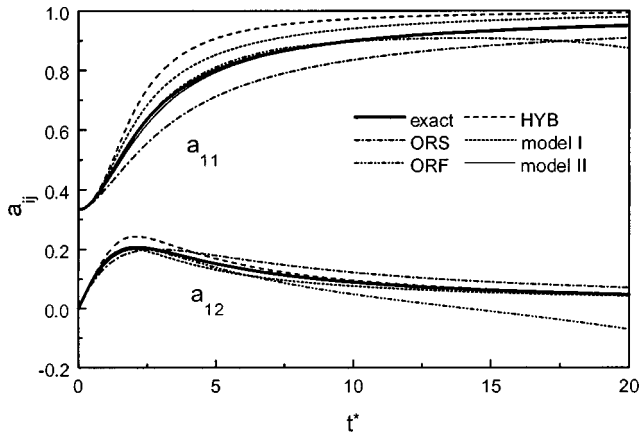

(a)

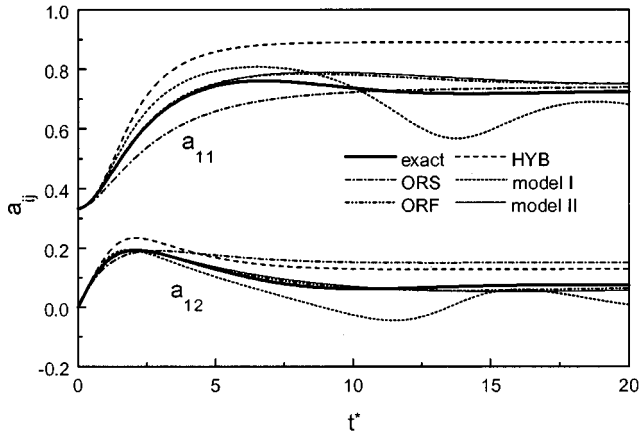

(b)

FIG. 5. Comparisons of a_{ij} between the exact solution and simulations based on various closure approximations for simple shear flow with (a) $C_I = 0$ and (b) $C_I = 0.01$.

closure approximations both transiently and steadily, while in Fig. 5(a) ORF can be seen to deviate from the exact value as time increases, indicating the beginning of oscillation. Also, model I can be seen to give better results than the HYB when $C_I = 0$, but oscillation occurs when $C_I = 0.01$.

For the simple shear flow, calculation results with different C_I values, namely, 0.001 and 0.1 are shown in Figs. 6(a) and 6(b), respectively. Only the ORF and model II are compared to the exact solution in Figs. 6(a) and 6(b). The results show that when $C_I = 0.001$, both the ORF and model II accurately follow the exact solution initially, but as time increases, model II has a maximum error of about 0.1 while the ORF starts to oscillate with a magnitude 0.15. Further calculations after $t^* = 40$ revealed that model II also oscillates for some time but with a smaller magnitude that eventually becomes steady. When $C_I = 0.1$, Fig. 6(b) shows that both the ORF and model II accurately predict the exact solution.

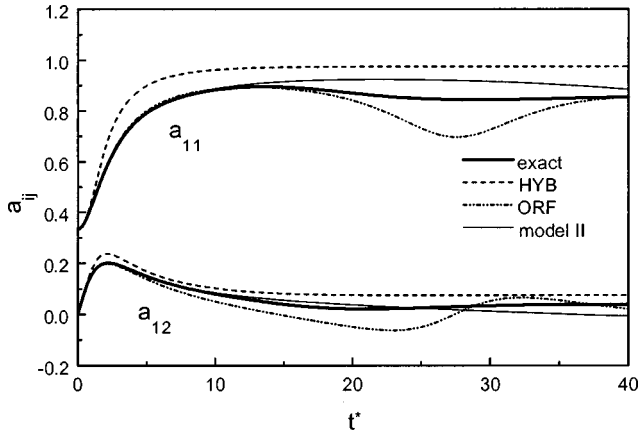

(a)

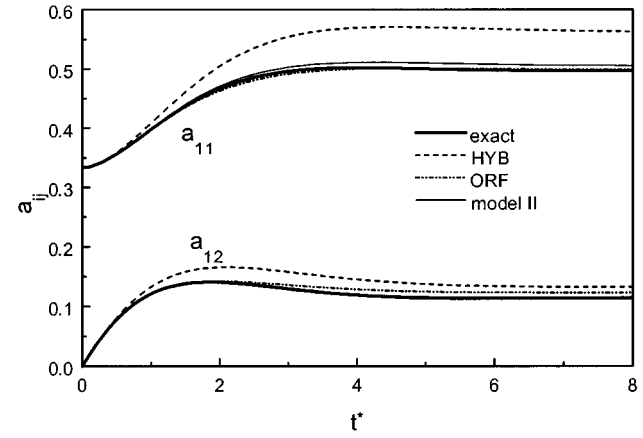

(b)

FIG. 6. Comparisons of a_{ij} between the exact solution and simulations based on various closure approximations for simple shear flow with (a) $C_I = 0.001$ and (b) $C_I = 0.1$.

Poor performance of the ORF at low C_I values is due to the fact that the ORF was obtained from the exact solution when $C_I = 0.01$. Thus, the fiber orientation prediction becomes inaccurate for other values of C_I. If the ORF was obtained by fitting the ODF at various C_I values, then this specific error might decrease, but the overall error for the general cases would most probably grow.

For a quantitative measure of the errors, the concept of average and steady errors was employed [Cintra and Tucker (1995)]. In this method, the scalar magnitude of errors at a given time is defined as follows:

$$e = \sqrt{(e_{ij}e_{ij})/2}, \quad \text{where} \quad e_{ij} = a_{ij}^{\text{exact}} - a_{ij}^{\text{closure}}. \tag{49}$$

The average and steady errors using the various closure approximations for the five homogeneous flow fields are summarized in Table V. For $C_I = 0.0$ and 0.001, the ORF shows oscillation behavior making the error values meaningless. Model II is very accu-

TABLE V. Average (avg) and steady (std) errors between orientation tensor computations using various closure approximations and exact solutions for homogeneous flow fields.

		HYB		ORF		Model II	
C_I	Flow	avg	std	avg	std	avg	std
	SS	0.050	0.023	0.134	0.070	0.005	0.005
	SSA	0.094	0.046	0.033	0.027	0.015	0.002
0.0	SSB	0.058	0.021	0.008	0.009	0.007	0.004
	UE	0.053	0.015	0.009	0.015	0.008	0.002
	BE	0.011	0.001	0.002	0.001	0.004	0.001
	SS	0.103	0.115	0.055	0.022	0.039	0.053
	SSA	0.068	0.006	0.034	0.003	0.014	0.010
0.001	SSB	0.034	0.003	0.008	0.004	0.004	0.002
	UE	0.031	0.003	0.009	0.005	0.004	0.002
	BE	0.010	0.001	0.003	0.002	0003	0.001
	SS	0.132	0.159	0.024	0.026	0.029	0.029
	SSA	0.057	0.034	0.013	0.015	0.030	0.037
0.01	SSB	0.035	0.003	0.004	0.002	0.006	0.010
	UE	0.032	0.003	0.004	0.004	0.005	0.008
	BE	0.013	0.006	0.003	0.004	0.003	0.003
	SS	0.050	0.060	0.007	0.009	0.006	0.008
	SSA	0.023	0.026	0.005	0.006	0.003	0.004
0.1	SSB	0.073	0.077	0.024	0.036	0.004	0.002
	UE	0.070	0.072	0.025	0.038	0.004	0.002
	BE	0.022	0.025	0.004	0.006	0.002	0.003

rate compared to the hybrid closure approximation for all cases and is equally or more accurate than the ORF depending on the C_I value. The only exception is the case of SSA at $C_I = 0.01$, where model II is less accurate than the ORF.

The results show that the HYB has some transient and steady-state errors, but it is a very stable approximation that never behaves nonphysically. Also, calculation by the HYB quickly reaches the steady state, which corresponds to a more aligned orientation state. The ORF can be seen to be more accurate than the HYB for $C_I = 0.01$, but for lower values of C_I the errors increase drastically. Thus, overall, it can be concluded that model II offers accurate solutions for a wide range of C_I values.

C. Nonhomogeneous flow fields

The first verification of fiber orientation calculations using the current closure approximations in nonhomogeneous flow fields was performed in the combined flow field represented by the following nondimensionalized velocity gradients [Cintra and Tucker (1995)]:

$$\left[\frac{\partial v_i}{\partial x_j}\right]^* = \begin{bmatrix} 0 & 1 & 0 \\ 0 & 0 & 0 \\ 0 & 0 & 0 \end{bmatrix} \quad \text{for} \quad 0 \leqslant t^* < 10, \tag{50}$$

$$\left[\frac{\partial v_i}{\partial x_j}\right]^* = \frac{1}{20}\begin{bmatrix} -1 & 0 & 0 \\ 0 & -1 & 20 \\ 0 & 0 & 2 \end{bmatrix} \quad \text{for} \quad 10 \leqslant t^* < 20, \tag{51}$$

TABLE VI. Average (avg) and maximum (max) errors between orientation tensor computations using various closure approximations and exact solutions for nonhomogeneous flow fields.

		HYB		ORF		Model II	
C_I	Flow	avg	max	avg	max	avg	max
0.0	Combined	0.078	0.206	0.026	0.066	0.005	0.015
	Disk ($z^* = 0.2$)	0.110	0.116	0.016	0.056	0.008	0.013
	Disk ($z^* = 0.5$)	0.061	0.063	0.217	0.348	0.015	0.017
	Disk ($z^* = 0.7$)	0.039	0.040	0.385	0.513	0.014	0.015
0.001	Combined	0.086	0.172	0.030	0.067	0.024	0.052
	Disk ($z^* = 0.2$)	0.097	0.118	0.042	0.141	0.005	0.009
	Disk ($z^* = 0.5$)	0.075	0.145	0.219	0.364	0.045	0.078
	Disk ($z^* = 0.7$)	0.151	0.219	0.245	0.332	0.063	0.093
0.01	Combined	0.086	0.154	0.017	0.045	0.025	0.063
	Disk ($z^* = 0.2$)	0.064	0.112	0.028	0.050	0.009	0.019
	Disk ($z^* = 0.5$)	0.103	0.179	0.013	0.021	0.029	0.034
	Disk ($z^* = 0.7$)	0.143	0.177	0.018	0.026	0.029	0.040
0.1	Combined	0.067	0.096	0.014	0.028	0.008	0.021
	Disk ($z^* = 0.2$)	0.039	0.064	0.009	0.011	0.006	0.007
	Disk ($z^* = 0.5$)	0.046	0.056	0.009	0.010	0.007	0.008
	Disk ($z^* = 0.7$)	0.052	0.058	0.010	0.010	0.008	0.009

$$\left[\frac{\partial v_i}{\partial x_j}\right]^* = \frac{1}{2}\begin{bmatrix} 2 & 0 & 0 \\ 0 & -1 & 2 \\ 0 & 0 & -1 \end{bmatrix} \quad \text{for} \quad 20 \leqslant t^* \leqslant 30. \tag{52}$$

The second test was performed for a center-gated disk flow in which the velocity field and velocity gradient are, respectively, given as follows:

$$v_r = \frac{3Q}{8\pi \cdot rb}\left(1-\frac{z^2}{b^2}\right) = \left(\frac{3Q}{8\pi \cdot b^2}\right)\frac{1}{r^*}[1-(z^*)^2], \quad v_\theta = v_z = 0, \tag{53}$$

$$\left[\frac{\partial v_i}{\partial x_j}\right] = \left(\frac{3Q}{8\pi \cdot b^3}\right)\frac{1}{(r^*)^2}\begin{bmatrix} -[1-(z^*)^2] & 0 & -2r^*z^* \\ 0 & [1-(z^*)^2] & 0 \\ 0 & 0 & 0 \end{bmatrix}, \tag{54}$$

where, Q and b are the volume flow rate and half-gap thickness, respectively, with $r^* = r/b$ and $z^* = z/b$. For simplification, the velocity field and time were nondimensionalized with the factor $3Q/8\pi b^3$ as the constant G in Eq. (47).

The detailed procedure for solving the orientation tensor in the center-gated disk flow is available in the literature [Altan and Rao (1995)]. In this study, the orientation tensors were calculated along the r direction at $z^* = 0.2$, 0.5, and 0.7.

The errors induced by the HYB, ORF, and model II in combined and center-gated disk flows are summarized in Table VI. As can be seen in Table VI, the results are similar to the case of homogeneous flows. As before, model II is more accurate than the HYB. The ORF oscillates when $C_I = 0$ or 0.001, and model II gives nearly the same results as the ORF when $C_I = 0$ or 0.01. The maximum error based on model II in the case of the combined flow occurred when $C_I = 0.01$, while for the center-gated disk flow it oc-

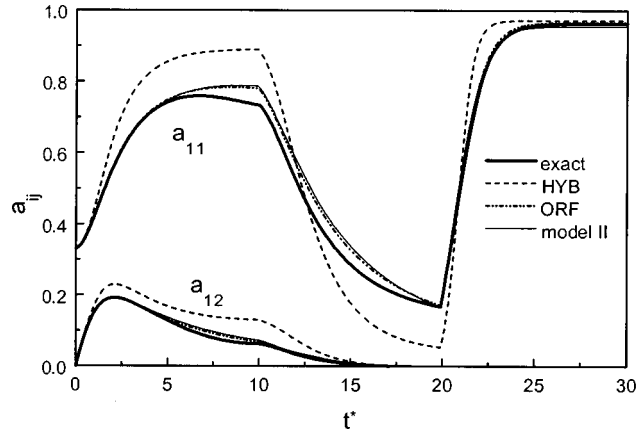

(a)

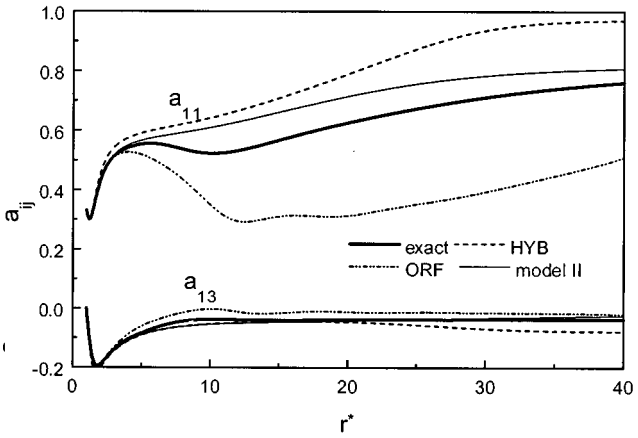

(b)

FIG. 7. Comparisons of a_{ij} between the exact solution and simulations based on the HYB; ORF, and model II for (a) combined flow with $C_I = 0.01$ and (b) center-gated disk flow at $z^* = 0.7$ with $C_I = 0.001$.

curred at $z^* = 0.7$ with $C_I = 0$. These two cases are shown in Fig. 7, and as can be seen, although the error values are maximum, model II tracks the variation reasonably well for both cases.

D. Contribution to extra stress

In the above verification tests, the flow fields were assumed to be independent of the fiber orientation. However, in reality extra stress is induced by the fiber orientation. Therefore, it must be checked whether the extra stress can be predicted accurately using the proposed closure approximations.

Considering the effects of fiber orientation, the stress equation can be written in the following form [Tucker (1991)]

$$\tau_{ij} = \eta_s \dot{\gamma}_{ij} + \eta_s c\{A\dot{\gamma}_{kl}a_{ijkl} + B(\dot{\gamma}_{ik}a_{kj} + a_{ik}\dot{\gamma}_{kj}) + C\dot{\gamma}_{ij} + 2Fa_{ij}D_r\}, \tag{55}$$

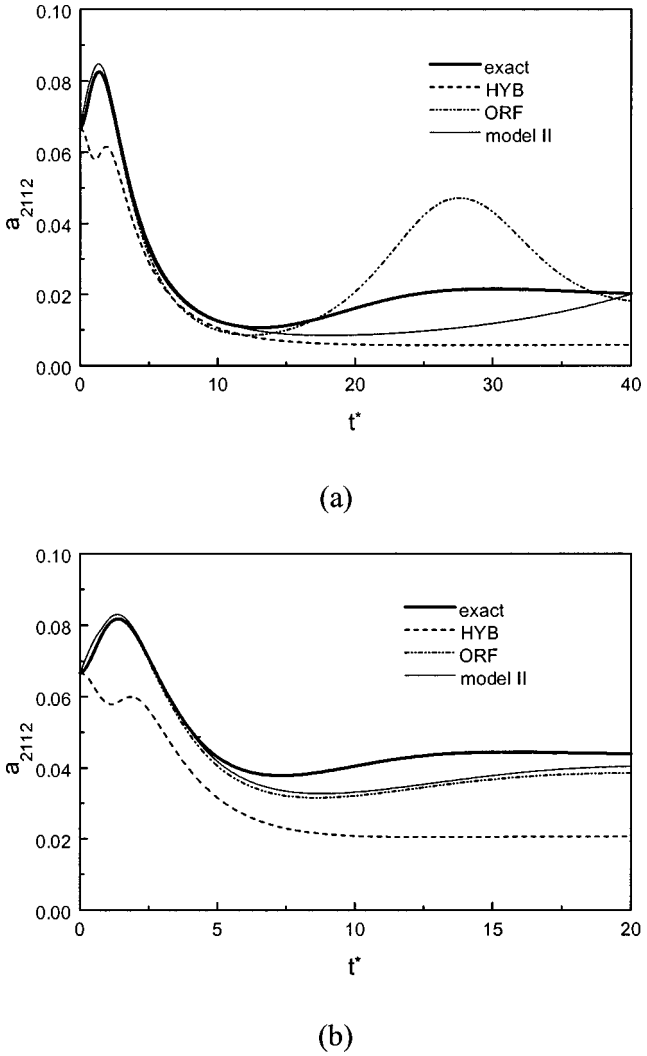

FIG. 8. Comparisons of a_{2112}, which denotes the contribution of extra stress induced by fiber orientation in total stress, between the exact solution and simulations based on various closure approximations for simple shear flow with (a) $C_I = 0.001$ and (b) $C_I = 0.1$.

where η_s is the solvent viscosity, c is the particle volume fraction, and A, B, C, and F are material constants. Since the fitting procedure used to obtain model II involved minimizing the errors of a_{ijkl} and model II was found to accurately predict a_{ij}, it is construed that the extra stress can be accurately predicted by using model II in solving the orientation tensor.

For example, in the coupled lubrication region, Eq. (55) can be simplified as

$$\tau_{2\alpha} = \eta_s \dot{\gamma}_{2\alpha} + 2\eta_s N_p \{\dot{\gamma}_{12} a_{2\alpha 12} + \dot{\gamma}_{32} a_{2\alpha 32}\} \quad (\alpha = 1,3), \tag{56}$$

where N_p is the material constant and the subscript 2 denotes the thickness direction. If simple shear flow is assumed in this case, the ratio of the extra stress becomes $2N_p a_{2112}$. The comparisons of a_{2112} between the exact solution and simulations based on the HYB, ORF, and model II for SS flow with $C_I = 0.001$ and 0.01 are shown in Figs. 8(a) and

8(b), respectively. The results show that model II is the most accurate and that it can be sufficiently used to predict the extra stress term.

E. Further requirements for the closure approximation

In the viewpoint of application, rather than accuracy stability is important because of the complex flow history. Recently, Edwards and Öttinger (1997) derived the necessary requirements for a closure approximation to behave physically from the time structure invariance criteria as follows:

$$a_{ijkl} \equiv a_{mn}\frac{\partial a_{ijkl}}{\partial a_{mn}}, \tag{57}$$

$$a_{njlm}\delta_{ki}-a_{ljkn}\delta_{im}+a_{inml}\delta_{jk}-a_{ilkn}\delta_{mj}+a_{ijmn}\delta_{lk}-a_{ijkl}\delta_{nm}+a_{lo}\frac{\partial a_{ijkn}}{\partial a_{mo}}-a_{no}\frac{\partial a_{ijml}}{\partial a_{ko}}$$

$$+a_{ol}\frac{\partial a_{ijkn}}{\partial a_{om}}-a_{on}\frac{\partial a_{ijml}}{\partial a_{ok}}+2a_{pokn}\frac{\partial a_{ijml}}{\partial a_{po}}-2a_{poml}\frac{\partial a_{ijkn}}{\partial a_{po}} = 0. \tag{58}$$

The natural closure approximation approximately satisfies Eq. (58) since it was constructed from analytic solutions when $C_I = 0$. Thus, it does not behave nonphysically as Cintra and Tucker (1995) have observed. However, the steady-state errors need to be reduced when $C_I > 0$. Both the ORF and model II do not satisfy these constraints, and so, nonphysical behavior may occur for these cases. However, the nonphysical behavior should be negligible for model II since it was fitted and verified using various C_I values. The fitting approach is a very efficient method to obtain quantitatively accurate closure approximations, but it is not easy to satisfy Eq. (58) simultaneously. Therefore, in order to obtain more accurate closure approximations, it may be viable to modify the existing stable closure approximations by fitting them to the DFCs.

The orthotropic property, inherent in the ORF and model II, is another limitation on the accuracy of the closure approximations. In general, the nonzero and nonorthotropic components of the fourth-order orientation tensor exist, and therefore, must be treated to further improve closure approximations.

Another critical point that should be mentioned is that the current orientation formulation relies on the Folgar and Tucker fiber-interaction model. If other fiber-interaction models are used, closure approximations proposed in this investigation might no longer guarantee its performance.

VI. CONCLUSIONS

In this investigation the modified hybrid closure approximation was constructed using the parametric form of the orientation distribution function which can accurately describe random-in-space, random-in-plane, and uniaxial distributions. Two parametric forms, model I and the ORS, were employed. Model I was assumed to be a simple distribution and the ORS is the linear interpolation of the three extremity cases. These two parametric forms were linearly interpolated to yield model II. The interpolating factor was obtained as a function of the interaction coefficient C_I by fitting the distribution function calculations.

Numerical tests were conducted in homogeneous flow fields as well as nonhomogeneous flow fields. It was found that model II gives good performance for a wide range of

C_I values without showing nonphysical behavior. Also, model II was used to accurately calculate the extra stress term for the given cases.

Although the currently developed modified hybrid closure approximation does not strictly satisfy the constraint equations (58), the present numerical simulations demonstrate reasonable physical behavior for the simulation flow fields considered. However, further investigation of the stability and accuracy of the current closure approximation is still helpful.

ACKNOWLEDGMENTS

The authors wish to thank the Korea Science and Engineering Foundation through the Engineering Research Center for Net Shape and Die Manufacturing at Pusan National University for a grant, under which this work was possible.

References

Advani, S. G. and C. L. Tucker III, ''The Use of Tensors to Describe and Predict Fiber Orientation in Short Fiber Composites,'' J. Rheol. **31**, 751–784 (1987).

Advani, S. G. and C. L. Tucker III, ''Closure Approximations for Three-Dimensional Structure Tensors,'' J. Rheol. **34**, 367–386 (1990).

Altan, M. C., S. Subbiah, S. I. Guceri, and R. B. Pipes, ''Numerical Prediction of Three-Dimensional Fiber Orientation in Hele–Shaw Flows,'' Polym. Eng. Sci. **30**, 848–859 (1990).

Altan, M. C. and B. N. Rao, ''Closed-Form Solution for the Orientation Field in a Center-Gated Disk,'' J. Rheol. **39**, 581–599 (1995).

Bay, R. S., Fiber Orientation in Injection Molded Composites: A Comparison of Theory and Experiments, Ph.D. thesis, Department of Mechanical and Industrial Engineering, University of Illinois, Urbana, IL (1991).

Bay, R. S. and C. L. Tucker III, ''Fiber Orientation in Simple Injection Moldings, Part 1: Theory and Numerical Methods,'' Polym. Compos. **13**, 317–321 (1992a).

Bay, R. S. and C. L. Tucker III, ''Fiber Orientation in Simple Injection Moldings, Part 2: Experimental Results,'' Polym. Compos. **13**, 322–342 (1992b).

Bretherton, F. P., ''The Motion of Rigid Particles in a Shear Flow at Low Reynolds Number,'' J. Fluid Mech. **14**, 284–304 (1962).

Chaubal, C. V. and L. G. Leal, ''A Closure Approximation for Liquid-Crystalline Polymer Models Based on Parametric Density Estimation,'' J. Rheol. **42**, 177–201 (1998).

Chung, S. T. and T. H. Kwon, ''Numerical Simulation of Fiber Orientation in Injection Molding of Short-Fiber-Reinforced Thermoplastics,'' Polym. Eng. Sci. **25**, 604–618 (1995).

Cintra, J. S. and C. L. Tucker III, ''Orthotropic Closure Approximation for Flow-Induced Fiber Orientation,'' J. Rheol. **39**, 1095–1122 (1995).

de Frahan, H. H., V. Verleye, F. Dupret, and M. J. Crochet, ''Numerical Prediction of Fiber Orientation in Injection Molding,'' Polym. Eng. Sci. **32**, 254–266 (1992).

Edwards, B. J. and H. C. Öttinger, ''Time-Structure Invariance Criteria for Closure Approximations,'' Phys. Rev. E **56**, 4097–4103 (1997).

Folgar, P. and C. L. Tucker III, ''Orientation Behavior of Fibers in Concentrated Suspensions,'' J. Reinf. Plast. Compos. **3**, 98–119 (1984).

Gupta, M. and K. K. Wang, ''Fiber Orientation and Mechanical Properties of Short-Fiber-Reinforced Injection-Molded Composites: Simulated and Experimental Results,'' Polym. Compos. **14**, 367–382 (1993).

Hand, G. L., ''Theory of Anisotropic Fluids,'' J. Fluid Mech. **13**, 33–46 (1962).

Jeffery, G. B., ''The Motion of Ellipsoidal Particles Immersed in a Viscous Fluid,'' Proc. R. Soc. London, Ser. A **102**, 161–179 (1922).

Ko, J. and J. R. Youn, ''Prediction of Fiber Orientation in the Thickness Plane During Flow Molding of Short Fiber Composites,'' Polym. Compos. **16**, 114–124 (1995).

Ranganathan, S. and S. G. Advani, ''A Simultaneous Solution for Flow and Fiber Orientation in Axisymmetric Diverging Radial Flow,'' J. Non-Newtonian Fluid Mech. **47**, 107–306 (1993).

Schieber, J. D., ''Internal Viscosity Dumbbell Model with a Gaussian Approximation,'' J. Rheol. **37**, 1003–1027 (1993).

Tucker III, C. L., ''Flow Regimes for Fiber Suspensions in Narrow Gaps,'' J. Non-Newtonian Fluid Mech. **39**, 239–268 (1991).

Tucker III, C. L. and S. G. Advani, ''Processing of Short-Fiber Systems,'' in *Flow and Rheology in Polymer Composites Manufacturing*, edited by S. G. Advani (Elsevier, Amsterdam, 1994), pp. 147–202.

Verley, V. and F. Dupret, ''Prediction of Fiber Orientation in Complex Injection Molded Parts,'' Proc. ASME Winter Annual Meeting, Nov. 28–Dec. 3, New Orleans, LA (1993).